

See discussions, stats, and author profiles for this publication at: <https://www.researchgate.net/publication/268804502>

Interferometric Plasmonic Lensing with Nanohole Arrays

ARTICLE *in* JOURNAL OF PHYSICAL CHEMISTRY LETTERS · NOVEMBER 2014

Impact Factor: 7.46 · DOI: 10.1021/jz502296n

CITATIONS

3

READS

35

4 AUTHORS, INCLUDING:



Yu Gong

City University of New York - Hunter College

26 PUBLICATIONS 118 CITATIONS

[SEE PROFILE](#)



Wayne Hess

Pacific Northwest National Laboratory

144 PUBLICATIONS 1,694 CITATIONS

[SEE PROFILE](#)

Interferometric Plasmonic Lensing with Nanohole Arrays

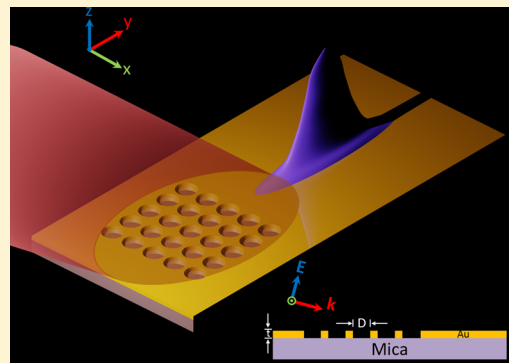
Yu Gong, Alan G. Joly, Patrick Z. El-Khoury, and Wayne P. Hess*

Physical Sciences Division, Pacific Northwest National Laboratory, P.O. Box 999, Richland, Washington 99352, United States

Supporting Information

ABSTRACT: Nonlinear photoemission electron microscopy (PEEM) of nanohole arrays in gold films is used to map propagating surface plasmons (PSPs) launched from lithographically patterned structures. Strong near-field photoemission patterns are observed in the PEEM images, recorded following low angle of incidence irradiation of nanohole arrays with sub-15 fs laser pulses centered at 780 nm. The recorded photoemission patterns are attributed to constructive and destructive interference between PSPs launched from the individual nanoholes which comprise the array. By exploiting the wave nature of PSPs, we demonstrate how varying the array geometry (hole diameter, pitch, and number of rows/columns) ultimately yields intense localized photoemission. Through a combination of PEEM experiments and finite-difference time-domain simulations, we identify the optimal array geometry for efficient light coupling and interferometric plasmonic lensing. We show a preliminary application of interferometric plasmonic lensing by enhancing the photoemission from the vertex of a gold triangle using a nanohole array.

SECTION: Plasmonics, Optical Materials, and Hard Matter



The resonant interaction between electromagnetic radiation and surface plasmon polaritons (SPPs) at the surface of noble metals is a subject of ever-growing interest. A long-standing goal, in this field, is to build a miniature all-plasmonic circuit featuring subcomponents operative beyond the diffraction limit of light.¹ To achieve this goal, exciting surface plasmon Eigenmodes is not the end game. Rather, the generated SPP waves need to be guided across the metal surface and ultimately decoupled into the next circuit component. In this regard, plasmonic lenses are attractive,^{2–10} as they can be used to couple light into a metal surface, to spatially guide propagating SPP waves, and to decouple the nascent surface waves into free space.¹¹ In this work, we combine nonlinear photoemission electron microscopy (PEEM) and finite-difference time-domain (FDTD) simulations to optimize light coupling and interferometric plasmonic lensing using arrays of nanoholes lithographically etched in gold thin films. Of the various techniques that have been applied to image SPPs,^{12–17} we use nonlinear PEEM to directly image the surface waves through photoemission^{18–20} rather than relying on molecular reporters in optical imaging schemes or tools of scanning probe microscopy.

Plasmonic lensing has been demonstrated using various constructs, including nanometric slit arrays,²¹ cross-shaped aperture arrays,²² and chirped circular nanoslits.²³ However, limited studies¹⁷ have been devoted to understanding the operative physics which governs plasmonic lensing using nanohole arrays in metal surfaces. This is somewhat surprising given the unique plasmonic properties of nanoholes and their arrays, which have been shown to exhibit extraordinary optical transmission^{24,25} and enhanced energy conversion when

coupled to photovoltaic devices²⁶ as well as high brightness photoemission.²⁷ Compared with previously described plasmonic lensing structures,^{3,8,9} the nanohole array design is more versatile for focusing electric fields in plasmonic integrated nanocircuits. We recently reported a nonlinear PEEM study of isolated nanoholes etched in gold thin films.²⁸ Damped elongated ring-like photoemission beat patterns following the low angle of incidence irradiation of the nanohole structures with sub-15 fs laser pulses centered at 780 nm were observed and associated with propagating SPPs launched from isolated nanoholes. A notable agreement between FDTD simulations and experiments corroborated our assignment of the observed photoemission patterns to SPPs launched from isolated nanoholes.²⁸ We also found that the efficiency of coupling light waves into isolated plasmonic holes can be controllably tuned by varying the diameter of the nanoholes.

The present work is motivated by the aforementioned results and takes advantage of the observations and assignments made therein.²⁸ In this study, we exploit the wave nature of the unidirectional SPPs launched from individual nanoholes of an array to optimize light coupling and interferometric plasmonic lensing. This is done by systematically varying the geometry of nanohole arrays (hole diameter, pitch, and number of rows/columns) etched in gold and directly visualizing the resulting spatial distribution of near-field intensity using nonlinear PEEM. Guided by experiments and FDTD simulations, we demonstrate 4-D control of the nanohole array plasmonic

Received: October 29, 2014

Accepted: November 21, 2014

Published: November 21, 2014

lensing by choice of center-to-center separation, laser wavelength, incident laser angle, and array row and column numbers. As an example, we show a preliminary application of enhanced photoemission from a gold triangle using nanohole array plasmonic lensing.

Figure 1 displays nonlinear PEEM maps of a single nanohole (800 nm diameter) and a 5×5 nanohole array (800 nm

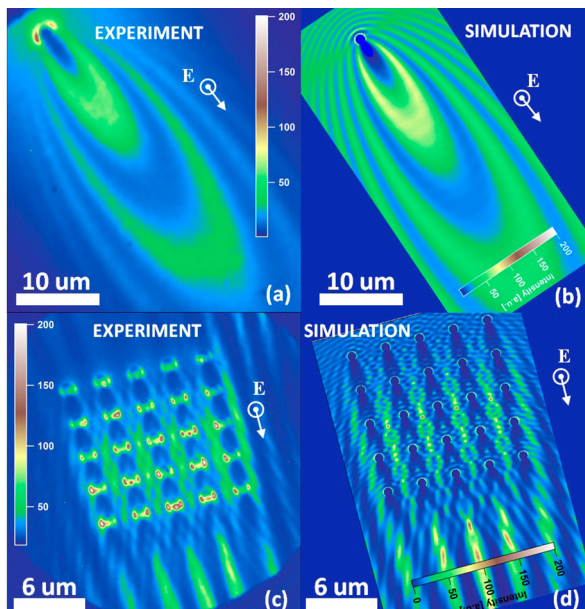


Figure 1. Comparison between the nonlinear PEEM images (a,c) and FDTD field intensity (E/E_0)⁶ maps (b,d) for a single nanohole (800 nm diameter) and a 5×5 nanohole array (800 nm diameter and 3000 nm separation). The incident 780 nm light source is p-polarized, with an electric field vector pointing out of the sample plane, as schematically illustrated in the insets. The calculated map of electric field enhancement pattern agrees well with the experimental nonlinear photoemission electron microscopy images.

diameter and 3000 nm separation) compared with their corresponding FDTD electric-field (E/E_0)⁶ enhancement maps. Both PEEM images were recorded following irradiation with p-polarized transform-limited (~15 fs pulse duration) laser pulses centered at 780 nm, incident onto the surface at an angle of 75° with respect to the surface normal. A plot of photoemission intensity versus laser power indicates a three-photon process (see the Supporting Information). As noted in prior analyses,^{29–31} the pulse effectively creates interference between a SPP and the same light source impinging on the surface surrounding the hole.

At least three photons are required to exceed the work function of the metal and hence to probe the polarization state prepared by the coupling structure (nanohole) through photoemission. Therefore, the photoemission intensity is proportional to the sixth power of the total polarization field integrated over time. The damped elongated ring-like photoemission beat patterns observed in the experimental PEEM (Figure 1a) and simulated FDTD (Figure 1b) images of the isolated nanohole are well-described in our previous study.²⁸ They are associated with propagating SPPs launched from the isolated plasmonic nanostructure. Similarly, the intense reticulated photoemission stripes observed in the experimental PEEM (Figure 1c) and simulated FDTD (Figure 1d) maps of the 5×5 nanohole array can be associated with propagating

SPPs. Specifically, these patterns arise from constructive and destructive interferences between the propagating surface waves launched from the individual nanoholes of the assembly excited at different time delays dependent on array position.

A remarkable overall agreement between the nonlinear PEEM and simulated FDTD maps is noted; see Figure 1c,d. The minor differences between experiment and theory can be readily attributed to imperfections in the lithographically patterned structures, which comprise efficient photoemission hot spots and lead to intense localized photoemission from the nanohole structures. Overall, the recorded nonlinear PEEM images of the array in concert with FDTD simulations together suggest that complex photoemission lensing patterns can be generated using plasmonic nanohole arrays. In the following, we exploit the wave nature of propagating SPPs to achieve various focused photoemission patterns through 2D SPP interferometry.

Figure 2 shows PEEM images of a series of 5×5 nanohole arrays with the center-to-center nanohole separation varied between 800 and 3000 nm and the nanohole diameter fixed at 600 nm. Intense photoemission is observed at the far side of

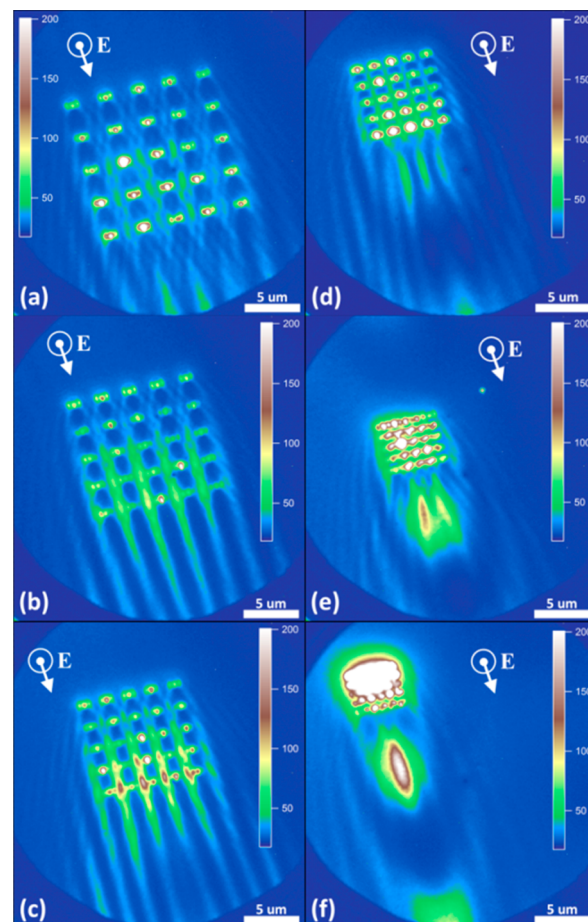


Figure 2. PEEM images of arrays (600 nm hole diameters throughout) featuring varying center-to-center separations of (a) 3000, (b) 2500, (c) 2000, (d) 1500, (e) 1000, and (f) 800 nm. The sample is irradiated with p-polarized, 780 nm femtosecond laser pulses. All of the images were time-integrated for 5 s using an average laser power ~80 mW. The laser propagation direction and polarization are indicated in the insets. The image intensity scale is set to reveal the highly localized photoemission regions (far side) on the metal surface, rendering the local photoemission in the nanohole region saturated in some images.

each array probed by nonlinear PEEM. The recorded images reveal that the photoemission pattern evolves from a striped pattern (Figure 2a) to a confined elliptical pattern (Figure 2f) as the center-to-center nanohole separation is decreased. Note that FDTD simulations again reproduce the measured photoemission patterns, thus corroborating the experimental results (see the Supporting Information). We find that the smallest nanohole separation (800 nm) yields an intense elliptical photoemission pattern focused on the far side of the array (Figure 2f).

In the focus region, the average photoemission yield is 70 times greater than its analogue measured from a flat gold substrate. In this context, focal length, f , is defined as the distance between the far-side (right) boundary of the nanohole array and the center (maximum intensity) of the focused elliptical photoemission beat pattern. To determine f , we consider regions in which the propagating SPP wave and light field are in phase (vide supra) such that $\Delta\varphi_{\text{SPP}} - \Delta\varphi_{\text{light}} = 2\pi$. As such, f is given by

$$f = \frac{\lambda_{\text{SPP}} \cdot \lambda_0}{\lambda_0 - \lambda_{\text{SPP}} \cdot \sin^3(\theta)} \quad (1)$$

where λ_0 is the laser wavelength, θ is the laser incidence angle with respect to the surface normal, and $\lambda_{\text{SPP}} = 2\pi/k_{\text{SPP}}$ is the wavelength of propagating SPP. The SPP wave vector is given by $k_{\text{SPP}} = Re[\omega(\epsilon_m/(1 + \epsilon_m)^{1/2}/c)]$, in which ϵ_m is the frequency-dependent dielectric of gold^{32–35} and ω denotes the frequency of the laser light. Given $\lambda_0 = 780$ nm, $\epsilon_m = -24.2 + 1.6i$,³² $\lambda_{\text{SPP}} = 763.7$ nm, and $\theta = 75^\circ$, we obtain $f \approx 5960$ nm. This is consistent with an experimentally measured value of 5940 nm (Figure 2f).

Figure 3 shows the FDTD calculated focal length (f) of the array as a function of laser wavelength and incidence angle. The

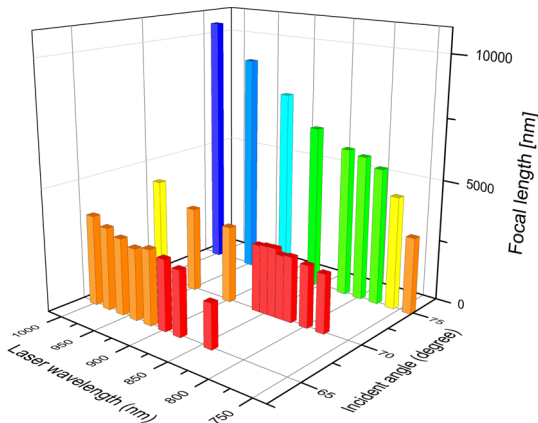


Figure 3. FDTD simulation of nanohole array focal length, featuring 800 nm nanohole separation (center-to-center) and 600 nm nanohole diameters, as a function of laser wavelength and angle of incidence.

FDTD simulations indicate that the SPP is not focused when the laser wavelength is below 840 nm for 65° incident angle and below 780 nm for 70° incident angle. Therefore, we do not include any data points in these regions. The focal length increases slowly with increasing laser wavelength but dramatically as a function of incident angle. The dielectric function of gold varies with wavelength. This affects the surface plasmon wave vector and in turn leads to a variation in the plasmonic lensing focal length at different laser wavelengths. The weak dependence on focal length arises because the gold

dielectric constant does not vary dramatically with wavelength. In contrast, the laser incident angle affects the interference of the light field and surface plasmon wave at the gold surface. This leads to a significant variation in the plasmonic lensing focal length because the focal length varies as the third power of the incident angle, as indicated in eq 1. Overall, our numerical simulations (see Figure 3) reveal that f can be tuned over a large range by adjusting both the laser incidence angle and excitation wavelength, aiding in the design of plasmon integrated nanocircuits.

To determine the dependence of the diffracted near field with respect to nanohole diameter, we fabricated nanohole arrays with the same center-to-center separation but different diameters. Figure 4 shows PEEM images of nanohole arrays

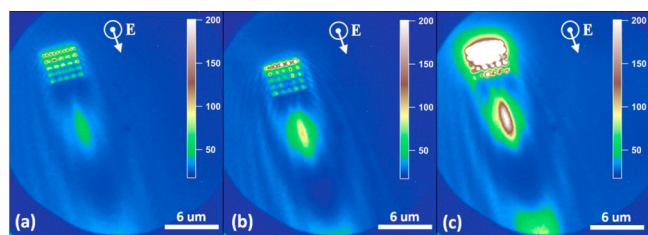


Figure 4. PEEM images of nanohole arrays with fixed nanohole separation (800 nm, center-to-center) but different nanohole diameters: (a) 200, (b) 400, (c) 600 nm. The sample is illuminated by p-polarized, 780 nm femtosecond laser pulses. The laser propagation direction and polarization are indicated in the insets.

with 800 nm center-to-center separation and three different nanohole diameters (200, 400, and 600 nm). The propagation direction and polarization of the 780 nm laser are again indicated by arrows. When the center-to-center separation in the nanohole array is fixed, variation of nanohole diameter affects the focal length only weakly (6.18, 6.06, and 5.94 μm). The photoemission intensity depends on nanohole diameter, as the coupling efficiency, and hence the attainable near field enhancement, is proportional to the laser-accessible inner surface area of the nanohole.²⁸ Therefore, photoemission intensity can be easily controlled by selecting nanohole diameter without strongly affecting the photoemission spatial distribution.

Figure 5 displays photoemission results from nanohole arrays with row and column numbers ($m \times n$, respectively) varied and center-to-center separation and diameter (1000 and 800 nm, respectively) fixed. The near-field photoemission pattern on the far side of the nanohole array evolves as a function of row number. Adding columns to the nanohole array increases the electric field coupling efficiency linearly along the laser propagation direction. In contrast, adding rows affects the plasmon interference at the surface, both in the parallel and perpendicular directions with respect to the laser propagation direction. In practice, this can be used to optimize plasmonic focusing. With this in mind, we constructed 25 arrays by varying row and column number from 1 to 5 (1 \times 1 to 5 \times 5), then measured their photoemission pattern and intensity. When we examine the results, we find that the 3 \times 5 nanohole array produces the most constricted focus (see Figure 5a,e) and highest intensity (see Figure 5g) of the diffracted near field photoemission.

We note that the k vector that best achieves SPP focusing does not necessarily provide the most efficient coupling for efficient SPP generation. The best focusing nanohole array has

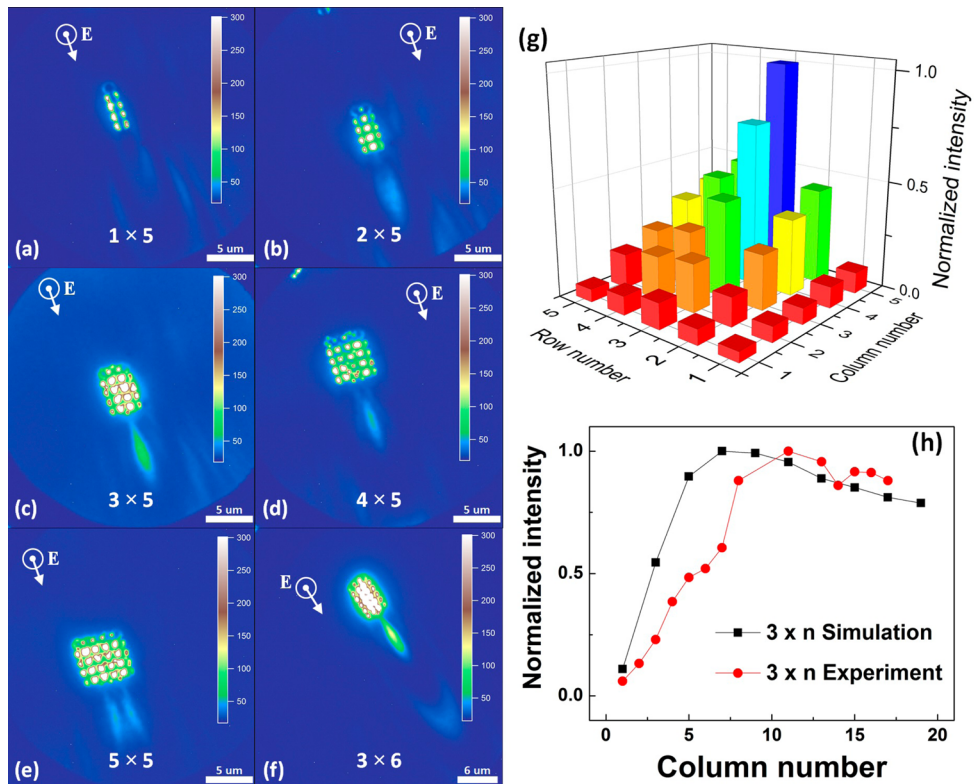


Figure 5. (a–f) PEEM images of $m \times n$ (row \times column) nanohole arrays with fixed center-to-center nanohole separation (1000 nm) and diameters (800 nm throughout). The sample is illuminated using p-polarized femtosecond laser pulses centered at 780 nm. The laser propagation direction and polarization are indicated in the insets. (f) PEEM image of a 3×6 nanohole array with 1000 nm nanohole separation and 800 nm nanohole diameters. (g) 3D plot of photoemission intensity as a function of m and n . (h) Experiment and simulation of normalized photoemission yield from nanohole arrays at the plasmonic focus as a function of increasing n .

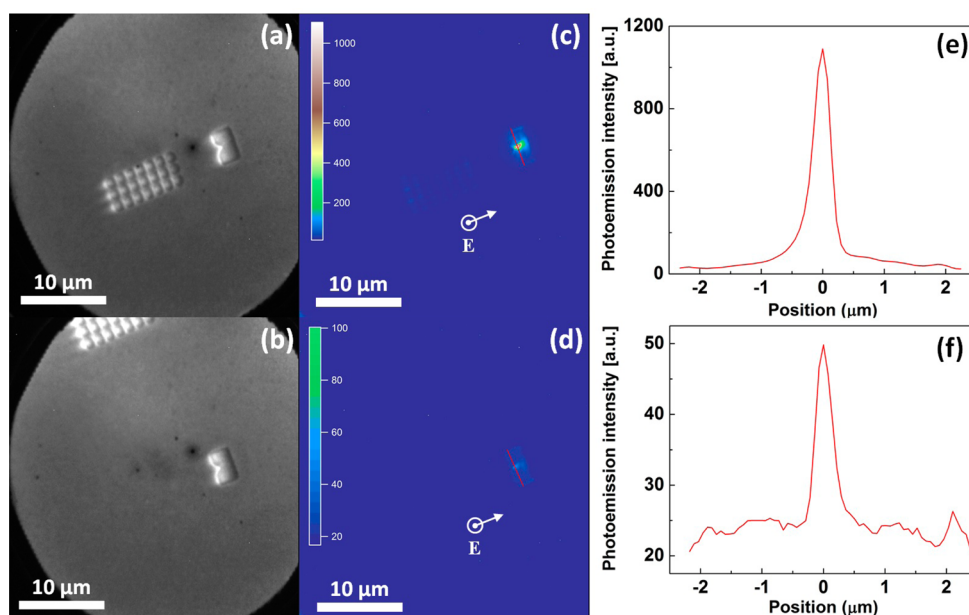


Figure 6. (a,b) PEEM images of a gold triangle with and without 3×7 (row \times column) nanohole array that has fixed center-to-center nanohole separation (1000 nm) and diameters (800 nm throughout). (c,d) Photoemission at the vertex of the gold triangle with and without the nanohole array. The sample is illuminated using p-polarized fs laser pulses centered at 780 nm. The laser propagation direction and polarization are indicated in the insets. (e,f) Photoemission intensity line profiles drawn perpendicular to the laser propagation direction as indicated by the red solid line in panels c and d.

800 nm hole separation, which has a k vector of $k_{800} = 2\pi/800$ nm $^{-1}$. This value is within 5% of the SPP k vector, $k_{\text{SPP}} = 2\pi/$

764 nm $^{-1}$. These k values are the most closely matched of all nanohole arrays considered. We note that perfectly matched k

vectors could possibly achieve even better coupling efficiency. We further note that increasing column number n does not alter the overall profile of the photoemission pattern but does increase photoemission intensity. (See Figure 5f.) This suggests that the focused photoemission intensity can be enhanced by adding columns to the array. We test this proposal in Figure 5h, where results from arrays featuring three rows and a variable number of columns are summarized. Our experiments qualitatively agree with the FDTD simulations that show the photoemission yield increases and then slightly decreases as a function of column number. However, experimentally the photoemission yield reaches maximum at larger column number than the corresponding FDTD simulation. This is likely a result of the finite experimental laser spot size. As the array size increases the new columns are not illuminated with maximum efficiency because the laser intensity is distributed in an elliptical Gaussian pattern due to the off-normal angle of incidence. In comparison, the FDTD calculations use a plane-wave illumination source and therefore each column sees the same illumination intensity.

Figure 6 displays a preliminary application of interferometric plasmonic lensing. We demonstrate enhanced photoemission from the vertex of a gold triangle. This is accomplished by etching a gold triangle at the interferometric focal point of a 3×7 nanohole array. The 3×7 nanohole array is designed to couple the incident laser field into the gold film and thus to generate a SPP wave that propagates and focuses at the vertex of the strategically placed nanotriangle. The sum of the focused SPP and the free-space laser field produces a much more intense field than what is observed from an identical isolated gold nanotriangle. Field focusing at the vertex of the nanotriangle greatly enhances the nonlinear photoemission process, indicative of an effective coupling between the plasmonic subcomponents of our model device. A UV lamp PEEM image of the sample is shown in Figure 6a. Under femtosecond laser illumination we observe strong photoemission at the vertex of this gold triangle (Figure 6c).

To demonstrate that the observed photoemission is due to coupling and focusing by the nanohole array, we display the photoemission intensity from an isolated gold triangle absent the nanohole array (Figure 6d). A UV lamp PEEM image of the isolated gold triangle is shown in Figure 6b. The photoemission intensity line profiles, at the vertex of the two samples, are plotted in Figure 6e,f. Compared with the gold triangle without nanohole array, the photoemission from the gold triangle with nanohole array is more intense by roughly a factor of 22. We tested five identically prepared structures, each of which produced similar results and an average photoemission intensity enhancement of 26 at the triangle tip. We therefore conclude that the photoemission at the gold triangle vertex is strongly enhanced by nanohole array coupling and plasmonic lensing. Our results will facilitate applications such as tip enhanced Raman for single molecule detection, design of plasmonic nanocircuits, and other plasmonic-resonance-based devices.

In summary, we probe propagating surface plasmons launched from nanohole arrays lithographically patterned in thin gold films through a unique combination of nonlinear PEEM and FDTD simulations. In examining the nanohole array geometry-dependent photoemission patterns, we find that (i) the launched propagating SPPs can be manipulated and focused by changing the separation between the nanoholes, (ii) the focal lengths of the array-based interferometric plasmonic lenses can be tuned by varying the incidence angle and

wavelength of the driving laser field, (iii) the overall efficiency of the lenses can be controlled by changing the nanohole diameters, and (iv) by varying the row and column numbers of the nanohole array, optimal interferometric focusing of propagating SPPs can be achieved. A preliminary application of nanohole array plasmonic lensing is demonstrated.

METHODS

The substrate consists of a 100 nm thick gold film sputtered on a freshly cleaved mica substrate. Nanohole arrays were milled into the gold film using focused ion beam lithography and imaged using a scanning electron microscope (FEI QUANTA 3D dual beam SEM/GaFIB). Different sets of 5×5 nanohole arrays were etched, featuring nanohole diameters varied between 100 and 1100 nm, and pitches varied between 800 and 3000 nm (SEM images shown in the Supporting Information). The samples were irradiated using a femtosecond titanium-sapphire oscillator (Griffin-10, KM Laboratories) operated at 90 MHz. Transform-limited (~ 15 fs) laser pulses centered at 780 nm were focused onto the sample surface (spot size $\sim 8 \times 10^{-3}$ mm 2) at an incidence angle of 75° from the surface normal, and the polarization of the laser was controlled using a half-wave plate. We chose gold for practical purposes. Gold has a long plasmon propagation distance, it does not tend to oxidize, and our 780 nm laser pulses efficiently excite its surface plasmon resonance. A photoemission electron microscope (Elmitec, PEEM III) was used to image laser-induced nonlinear photoemission from the sample. The nascent photoelectrons were accelerated from the sample surface toward an electrically grounded objective lens in a 10 V/ μ m electric field, further focused using a series of magneto-optic lenses, and projected onto a microchannel plate/phosphor screen imaging stack. A computer controlled charged coupled device camera captures the images from the phosphor screen. The base pressure of the microscope chamber is maintained at $\sim 9 \times 10^{-11}$ and increases to $\sim 7 \times 10^{-10}$ Torr throughout the measurements.

Numerical simulations were performed using a commercial FDTD package (Lumerical FDTD Solutions). The interaction of electromagnetic plane waves with an individual nanohole is calculated by iteratively solving finite-difference analogues of the time-dependent Maxwell equations. The iterative process is repeated until the desired transient or steady-state electromagnetic field behavior is well-resolved. The sample and experimental geometries are identical to their experimental analogues. The dielectric permittivity of gold is taken from Johnson and Christy.³²

ASSOCIATED CONTENT

Supporting Information

SEM image of a 5×5 nanohole array. Photoemission intensity as a function of laser intensity. FDTD surface field intensity maps of nanohole array with 600 nm diameter but different center-to-center separations. This material is available free of charge via the Internet at <http://pubs.acs.org>.

AUTHOR INFORMATION

Corresponding Author

*E-mail: wayne.hess@pnnl.gov.

Notes

The authors declare no competing financial interest.

ACKNOWLEDGMENTS

This work was supported by the U.S. Department of Energy, Office of Science, Office of Basic Energy Sciences, Division of Chemical Sciences, Geosciences & Biosciences. P.Z.E.-K. acknowledges support from the Laboratory Directed Research and Development Program through a Linus Pauling Fellowship at Pacific Northwest National Laboratory (PNNL), a multi-program national laboratory operated for DOE by Battelle. The research was performed using EMSL, a national scientific user facility sponsored by the Department of Energy's Office of Biological and Environmental Research and located at PNNL.

REFERENCES

- (1) Ebbesen, T. W.; Genet, C.; Bozhevolnyi, S. I. Surface-Plasmon Circuitry. *Phys. Today*. **2008**, *61*, 44–50.
- (2) Lerman, G. M.; Yanai, A.; Levy, U. Demonstration of Nanofocusing by the Use of Plasmonic Lens Illuminated with Radially Polarized Light. *Nano Lett.* **2009**, *9*, 2139–2143.
- (3) Yin, L. L.; Vlasko-Vlasov, V. K.; Pearson, J.; Hiller, J. M.; Hua, J.; Welp, U.; Brown, D. E.; Kimball, C. W. Subwavelength Focusing and Guiding of Surface Plasmons. *Nano Lett.* **2005**, *5*, 1399–1402.
- (4) Evlyukhin, A. B.; Bozhevolnyi, S. I.; Stepanov, A. L.; Kiyan, R.; Reinhardt, C.; Passinger, S.; Chichkov, B. N. Focusing and Directing of Surface Plasmon Polaritons by Curved Chains of Nanoparticles. *Opt. Express*. **2007**, *15*, 16667–16680.
- (5) Yang, S. Y.; Chen, W. B.; Nelson, R. L.; Zhan, Q. W. Miniature Circular Polarization Analyzer with Spiral Plasmonic Lens. *Opt. Lett.* **2009**, *34*, 3047–3049.
- (6) Chen, W. B.; Abeysinghe, D. C.; Nelson, R. L.; Zhan, Q. W. Experimental Confirmation of Miniature Spiral Plasmonic Lens as a Circular Polarization Analyzer. *Nano Lett.* **2010**, *10*, 2075–2079.
- (7) Chen, W. B.; Abeysinghe, D. C.; Nelson, R. L.; Zhan, Q. W. Plasmonic Lens Made of Multiple Concentric Metallic Rings under Radially Polarized Illumination. *Nano Lett.* **2009**, *9*, 4320–4325.
- (8) Wang, L. M.; Petek, H. Focusing Surface Plasmon Polariton Wave Packets in Space and Time. *Laser Photonics Rev.* **2013**, *7*, 1003–1009.
- (9) Lemke, C.; Schneider, C.; Leissner, T.; Bayer, D.; Radke, J. W.; Fischer, A.; Melchior, P.; Evlyukhin, A. B.; Chichkov, B. N.; Reinhardt, C.; et al. Spatiotemporal Characterization of SPP Pulse Propagation in Two-Dimensional Plasmonic Focusing Devices. *Nano Lett.* **2013**, *13*, 1053–1058.
- (10) Liu, Z. W.; Steele, J. M.; Srituravanich, W.; Pikus, Y.; Sun, C.; Zhang, X. Focusing Surface Plasmons with a Plasmonic Lens. *Nano Lett.* **2005**, *5*, 1726–1729.
- (11) Lopez-Tejeira, F.; Rodrigo, S. G.; Martin-Moreno, L.; Garcia-Vidal, F. J.; Devaux, E.; Ebbesen, T. W.; Krenn, J. R.; Radko, I. P.; Bozhevolnyi, S. I.; Gonzalez, M. U.; et al. Efficient Unidirectional Nanoslit Couplers for Surface Plasmons. *Nat. Phys.* **2007**, *3*, 324–328.
- (12) Chang, W. S.; Lassiter, J. B.; Swanglap, P.; Sobhani, H.; Khatua, S.; Nordlander, P.; Halas, N. J.; Link, S. A Plasmonic Fano Switch. *Nano Lett.* **2012**, *12*, 4977–4982.
- (13) Wild, B.; Cao, L. N.; Sun, Y. G.; Khanal, B. P.; Zubarev, E. R.; Gray, S. K.; Scherer, N. F.; Pelton, M. Propagation Lengths and Group Velocities of Plasmons in Chemically Synthesized Gold and Silver Nanowires. *ACS Nano*. **2012**, *6*, 472–482.
- (14) Solis, D.; Paul, A.; Chang, W. S.; Link, S. Mechanistic Study of Bleach-Imaged Plasmon Propagation (Blipp). *J. Phys. Chem. B* **2013**, *117*, 4611–4617.
- (15) Nauert, S.; Paul, A.; Zhen, Y. R.; Solis, D.; Vigderman, L.; Chang, W. S.; Zubarev, E. R.; Nordlander, P.; Link, S. Influence of Cross Sectional Geometry on Surface Plasmon Polariton Propagation in Gold Nanowires. *ACS Nano*. **2014**, *8*, 527–580.
- (16) Liu, X. J.; Wang, Y.; Potma, E. O. A Dual-Color Plasmonic Focus for Surface-Selective Four-Wave Mixing. *Appl. Phys. Lett.* **2012**, *101*, 081116.
- (17) Egorov, D.; Dennis, B. S.; Blumberg, G.; HafTEL, M. I. Two-Dimensional Control of Surface Plasmons and Directional Beaming from Arrays of Subwavelength Apertures. *Phys. Rev. B* **2004**, *70*, 033404.
- (18) Peppernick, S. J.; Joly, A. G.; Beck, K. M.; Hess, W. P. Plasmonic Field Enhancement of Individual Nanoparticles by Correlated Scanning and Photoemission Electron Microscopy. *J. Chem. Phys.* **2011**, *134*, 034507.
- (19) Peppernick, S. J.; Joly, A. G.; Beck, K. M.; Hess, W. P. Near-Field Focused Photoemission from Polystyrene Microspheres Studied with Photoemission Electron Microscopy. *J. Chem. Phys.* **2012**, *137*, 014202.
- (20) Xiong, G.; Shao, R.; Droubay, T. C.; Joly, A. G.; Beck, K. M.; Chambers, S. A.; Hess, W. P. Photoemission Electron Microscopy of TiO₂ Anatase Films Embedded with Rutile Nanocrystals. *Adv. Funct. Mater.* **2007**, *17*, 2133–2138.
- (21) Verslegers, L.; Catrysse, P. B.; Yu, Z. F.; White, J. S.; Barnard, E. S.; Brongersma, M. L.; Fan, S. H. Planar Lenses Based on Nanoscale Slit Arrays in a Metallic Film. *Nano Lett.* **2009**, *9*, 235–238.
- (22) Lin, L.; Goh, X. M.; McGuinness, L. P.; Roberts, A. Plasmonic Lenses Formed by Two-Dimensional Nanometric Cross-Shaped Aperture Arrays for Fresnel-Region Focusing. *Nano Lett.* **2010**, *10*, 1936–1940.
- (23) Fu, Y. Q.; Liu, Y.; Zhou, X. L.; Xu, Z. W.; Fang, F. Z. Experimental Investigation of Superfocusing of Plasmonic Lens with Chirped Circular Nanoslits. *Opt. Express*. **2010**, *18*, 3438–3443.
- (24) Ghaemi, H. F.; Thio, T.; Grupp, D. E.; Ebbesen, T. W.; Lezec, H. J. Surface Plasmons Enhance Optical Transmission through Subwavelength Holes. *Phys. Rev. B* **1998**, *58*, 6779–6782.
- (25) Ebbesen, T. W.; Lezec, H. J.; Ghaemi, H. F.; Thio, T.; Wolff, P. A. Extraordinary Optical Transmission through Sub-Wavelength Hole Arrays. *Nature* **1998**, *391*, 667–669.
- (26) Li, J. T.; Cushing, S. K.; Zheng, P.; Meng, F. K.; Chu, D.; Wu, N. Q. Plasmon-Induced Photonic and Energy-Transfer Enhancement of Solar Water Splitting by a Hematite Nanorod Array. *Nat. Commun.* **2013**, *4*, 3651.
- (27) Li, R. K.; To, H.; Andonian, G.; Feng, J.; Polyakov, A.; Scoby, C. M.; Thompson, K.; Wan, W.; Padmore, H. A.; Musumeci, P. Surface-Plasmon Resonance-Enhanced Multiphoton Emission of High-Brightness Electron Beams from a Nanostructured Copper Cathode. *Phys. Rev. Lett.* **2013**, *110*, 074801.
- (28) Gong, Y.; Joly, A. G.; El-Khoury, P. Z.; Hess, W. P. Nonlinear Photoemission Electron Micrographs of Plasmonic Nanoholes in Gold Thin Films. *J. Phys. Chem. C* **2014**, *118*, 25671–25676.
- (29) Kubo, A.; Pontius, N.; Petek, H. Femtosecond Microscopy of Surface Plasmon Polariton Wave Packet Evolution at the Silver/Vacuum Interface. *Nano. Lett.* **2007**, *7*, 470–475.
- (30) Zhang, L. X.; Kubo, A.; Wang, L. M.; Petek, H.; Seideman, T. Imaging of Surface Plasmon Polariton Fields Excited at a Nanometer-Scale Slit. *Phys. Rev. B* **2011**, *84*, 245442.
- (31) Zhang, L. X.; Kubo, A.; Wang, L. M.; Petek, H.; Seideman, T. Universal Aspects of Ultrafast Optical Pulse Scattering by a Nanoscale Asperity. *J. Phys. Chem. C* **2013**, *117*, 18648–18652.
- (32) Johnson, P. B.; Christy, R. W. Optical Constants of Noble Metals. *Phys. Rev. B* **1972**, *6*, 4370.
- (33) Fowler, R. H. The Analysis of Photoelectric Sensitivity Curves for Clean Metals at Various Temperatures. *Phys. Rev.* **1931**, *38*, 45.
- (34) DuBridge, L. A. Theory of the Energy Distribution of Photoelectrons. *Phys. Rev.* **1933**, *43*, 0727.
- (35) Musumeci, P.; Cultrera, L.; Ferrario, M.; Filippetto, D.; Gatti, G.; Gutierrez, M. S.; Moody, J. T.; Moore, N.; Rosenzweig, J. B.; Scoby, C. M.; et al. Multiphoton Photoemission from a Copper Cathode Illuminated by Ultrashort Laser Pulses in an RF Photoinjector. *Phys. Rev. Lett.* **2010**, *104*, 084801.